Supplementary Information

Tuning the d-Band States of NiFe-MOFs by Combining Early and Late Transition Metal for Enhanced Electrocatalytic Oxygen Evolution

Dan Wen[a], Dongling Xie[a], Bo Huang[a], Qiuping Huang[a], Dunmin Lin[a], Chenggang Xu[a], Fengyu Xie[a]*, Guangzhao Wang[b]* Wenhan Guo[c]*

[a] College of Chemistry and Materials Science, Sichuan Normal University, Chengdu, 610066, China.

[b] Key Laboratory of Extraordinary Bond Engineering and Advanced Materials Technology of Chongqing, School of Electronic Information Engineering, Yangtze Normal University, Chongqing, 408100, China.

[c] School of Physical Science, Great Bay University, Dongguan, Guangdong, 523000, China.

*Corresponding author(s). E-mail: [*] xiefengyu161@163.com

wangyan6930@126.com

whguo@gbu.edu.cn

Experimental

Reagents and materials

All chemical regents were analytically pure. Nickel foam (NF; area: 2 cm × 3 cm) was bought from Shenzhen Yunfei Materials Co., Ltd. Ferric chloride hexahydrate ($Fe(NO_3)_3·9H_2O$; Aladdin), Chromic nitrate nonahydrate ($Cr(NO_3)_3·9H_2O$; Tianjin Anjirui Chemical Company), terephthalic acid ($C_8H_6O_4$, TPA; Shanghai Maclin Biochemical Technology Co., Ltd), N,N-dimethylformamide (DMF; Chengdu Haijun Chemical Co., Ltd), ethanol and deionized water were used.

Preparation of NiFe-MOF

Firstly, 0.4040 g (1 mmol) of $Fe(NO_3)_3·9H_2O$ and 0.4983 g (3 mmol) of TPA were added to 35 mL of DMF. The solution was stirred for 15 minutes and added 2.5 mL ethanol and 2.5 mL deionized water successively. Next, the mixed solution was stirred for 30 minutes before pouring into a 50 ml autoclave. Before closing the reaction kettle, nickel foam (2 × 3 cm) treated with hydrochloric acid (4 mol L^{-1}) was added as the nickel source. At last, the reaction kettle was placed in an oven at 125℃ for 12 hours, and then it was naturally cooled down to room temperature. The material was rinsed several times with DMF, ethanol and deionized water sequentially, and then in a vacuum oven at 60 ℃ overnight to dry.

Preparation of Cr-NiFe-MOF

The synthesis method of Cr-NiFe-MOF was similar to the above-mentioned process, and 0.1200 g (0.3 mmol) $Cr(NO_3)_3·9H_2O$ was doped in the homogeneous solution.

Characterizations

Powder X-ray diffraction (PXRD) data were acquired from a LabX XRD-6100 X-ray diffractometer with Cu Kα radiation (40 kV, 30 mA) and a 0.154 nm wavelength (Shimadzu, Osaka, Japan) within the range of 2θ = 5~60°. Fourier transform infrared (FT-IR) was carried out on an FTIR spectrometer (Theromo Nicolet Corporation, Madison, WI, USA) using the potassium bromide pellet method at an ambient temperature. Raman measurements were conducted on a Renishaw Invia spectrometer (Renishaw Company, Gloucestershire, England). The thermal behaviour was carried out on a thermogravimetric weight analysis (TGA) instrument (METTLER TOLEDO TGA2 thermogravimetric analyzer). Scanning electron microscope (SEM) images were obtained using a XL30 ESEM FEG at a 20 kV accelerating voltage. The transmission electron microscope (TEM) and energy dispersive X-Ray (EDX) data were collected using a FEI Tecnai G2 F20 (FEI Company, Hillsboro, OR, USA) and OXFORD X-max 80T (FEI Company, Hillsboro, OR, USA). A Thermo Scientifific K-Alpha X-ray photoelectron spectrometer (Thermo Fisher Scientifific, Waltham, MA, USA) using Al was used to acquire X-ray photoelectron spectroscopy (XPS) spectra. Ultraviolet photoemission spectroscopy (UPS) was carried out in an UHV surface analysis system (Thermo ESCALAB XI+) with a monochromatic He light source (21.22 eV), consisting of an entry chamber (base pressure ≈2×10-10 mbar), a preparation chamber (≈8×10-10 mbar) and an analysis chamber (≈2×10-10 mbar).

Electrochemical Measurements

All electrochemical performance was measured in a three-electrode system using an electrochemical workstation (CHI 660E) in 1.0 M KOH solution at room temperature. The working electrode was Cr-NiFe-MOF or NiFe-MOF, the counter electrode was a graphite plate, and Hg/HgO electrode was used as the reference. Each potential was reported as one form of reversible hydrogen electrode (RHE), calculated as follows:

$$E_{(RHE)} = E_{(Hg/HgO)} + (0.098 + 0.059\ pH)\ V$$

Electrochemical surface area (ECSA)

Electrochemical surface areas (ECSAs) were evaluated by measuring the double-layer capacitance (C_{dl}) via CV. CV curves were measured at various scan rates from 20 to 100 mV s^{-1} under the potential window from 0.21 to 0.31 V. According to the following equation, the ECSAs of the series catalysts were calculated:

$$\mathrm{ECSA} = \frac{C_{dl}}{C_s}$$

where C_s is the specific capacitance per unit area for samples under identical electrolyte conditions. For our estimates of surface area, we used the general specific capacitances of C_s =0.040 mF·cm^{-2} in 1.0 M KOH. The ECSA-normalized current density for as-prepared catalysts was calculated by:[1]

$$\text{ECSA-normalized current density} = \text{current density} \times \text{ECSA}$$

Turnover frequency (TOF) test

Turnover frequency (TOF) can be calculated to further estimate the intrinsic activity of catalysts, which follows the equation:

$$\mathrm{TOF} = \frac{J \times A}{4 \times F \times \mathrm{m}}$$

where J is the current density (A cm^{-2}) at a given overpotential of 0.30 V, A and m are the area of the electrode (0.25 cm^{-2}) and the number of loading moles of the active substance on the substrate, respectively. The number 4 represents a four-electron transfer process of OER. F is the Faraday constant (96,485 C mol^{-1}).

Electrochemical stability test

The long-term durability of Cr-NiFe-MOF was assessed by i-t test in 1 M potassium hydroxide solution. Voltage of 1.47 V was provided to achieve current densities close to 100 mA cm^{-2} to further understand the stability of the material at high current densities.

Faraday electrochemical measurement

The three-electrode system was measured using a CHI 660E electrochemical analyzer. Cr-NiFe-MOF was the working electrode, Hg/HgO was the reference electrode and graphite rod was the counter electrode. A 5 mL measuring cylinder was used to collect oxygen precipitation on the working electrode during the test by drainage method. And the Faraday efficiency of OER was calculated by recording the time required for the precipitation of the same volume of oxygen. The current density was constant at 100 mA cm^{-2} during the test.

Calculation method

The present first principle DFT calculations were performed by Vienna Ab initio Simulation Package(VASP) with the projector augmented wave (PAW) method.[2,3] The exchange-functional was treated using the generalized gradient approximation (GGA) of Perdew-Burke-Ernzerhof (PBE) functional.[4] The Spin-polarizations were carried out for all calculations. The energy cutoff for the plane wave basis expansion was set to 450 eV and the force on each atom less than 0.02 eV/Å was set for convergence criterion of geometry relaxation. The Brillouin-zone integration was sampled by single Γ point. The self-consistent calculations applied a convergence energy threshold of 10-5 eV. The DFT-D3 method was employed to consider the van der Waals interaction.[5] The computational model of NiFe-MOF and Cr-NiFe-MOF were constructed based on a 1×2×1 supercell.

The free energies of the OER steps are calculated using the equation:[6]

$$\Delta G = \Delta E_{DFT} + \Delta E_{ZPE} - T\Delta S$$

where ΔE_{DFT} is the DFT energy difference, and the ΔE_{ZPE} and $T\Delta S$ terms are obtained based on vibration analysis.

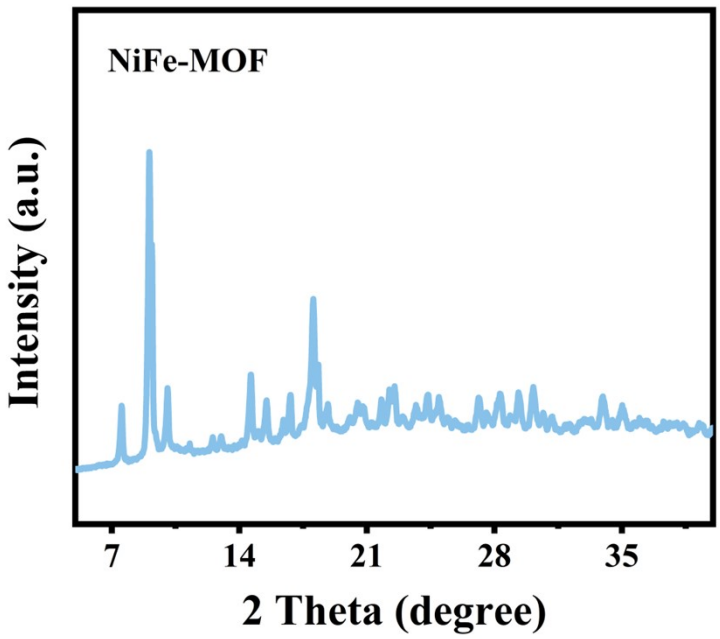

Fig. S1 XRD spectrum of NiFe-MOF.

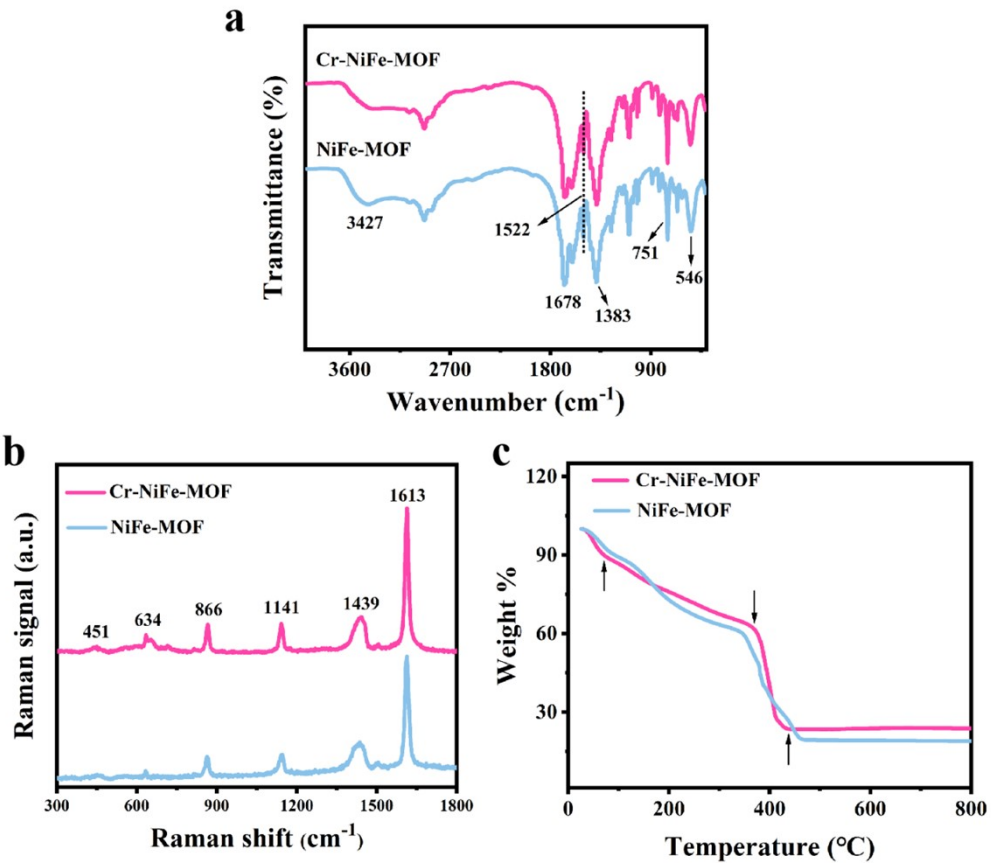

Fig. S2 (a) FT-IR spectra, (b) Raman spectra and (c) TGA spectra for NiFe-MOF and Cr-NiFe-MOF.

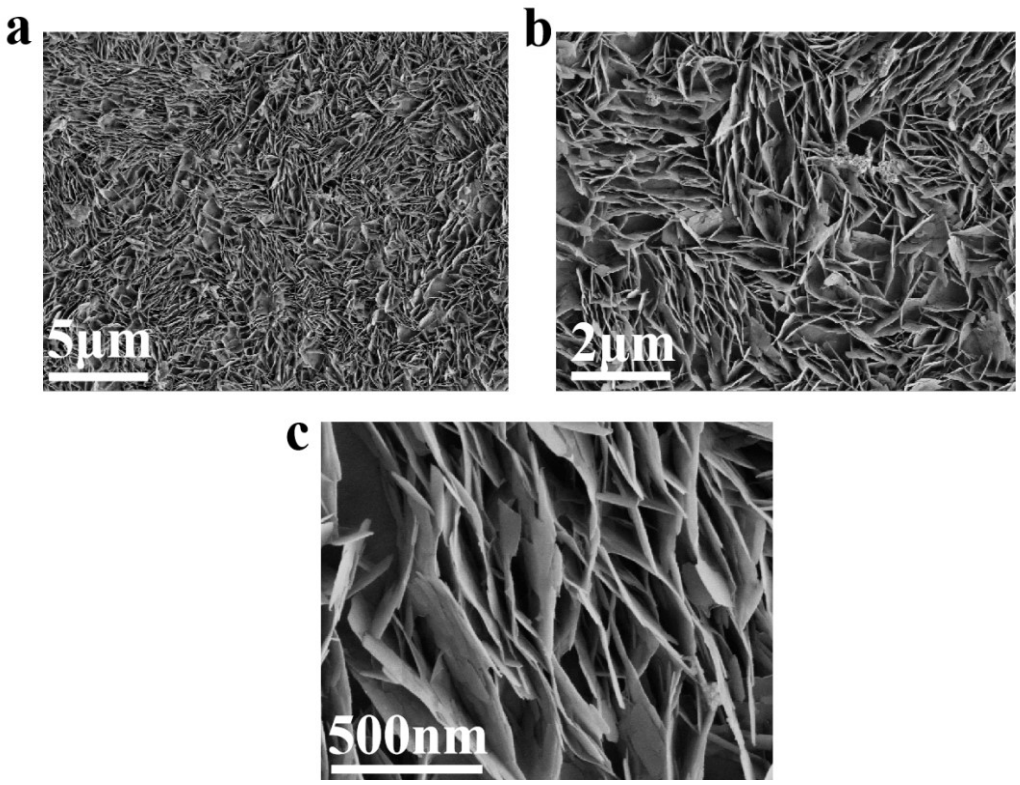

Fig. S3 SEM spectra of NiFe-MOF.

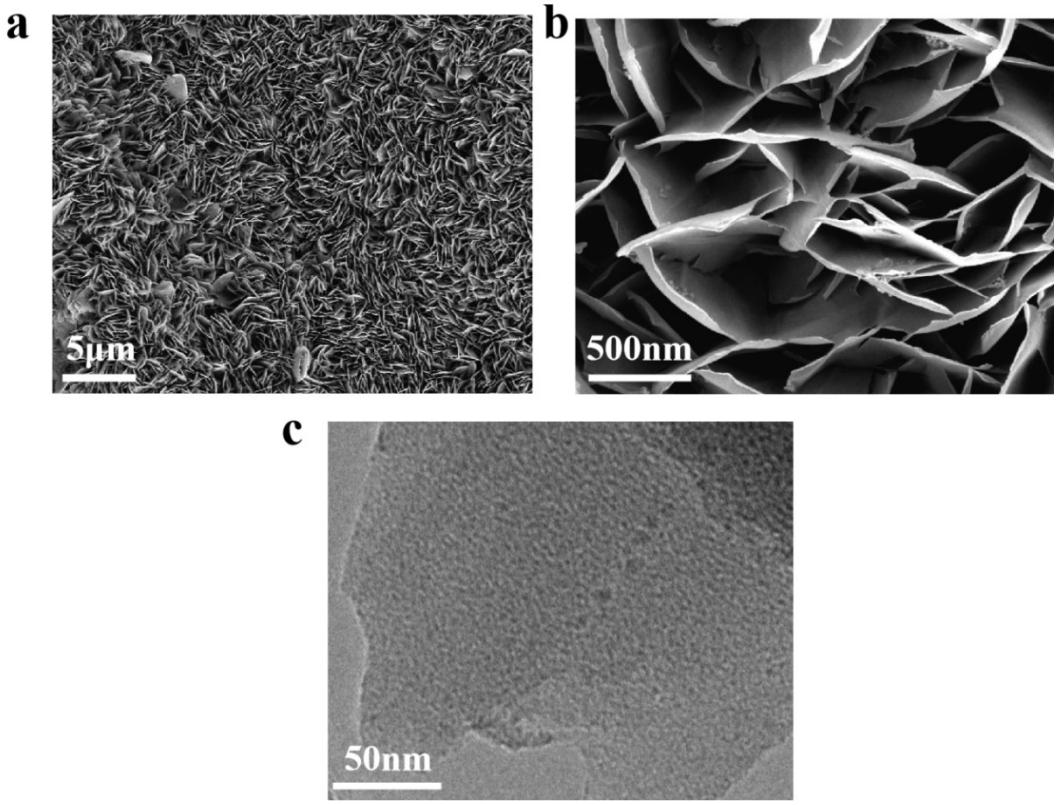

Fig. S4 (a,b) SEM spectra and (c) TEM spectrum of Cr-NiFe-MOF.

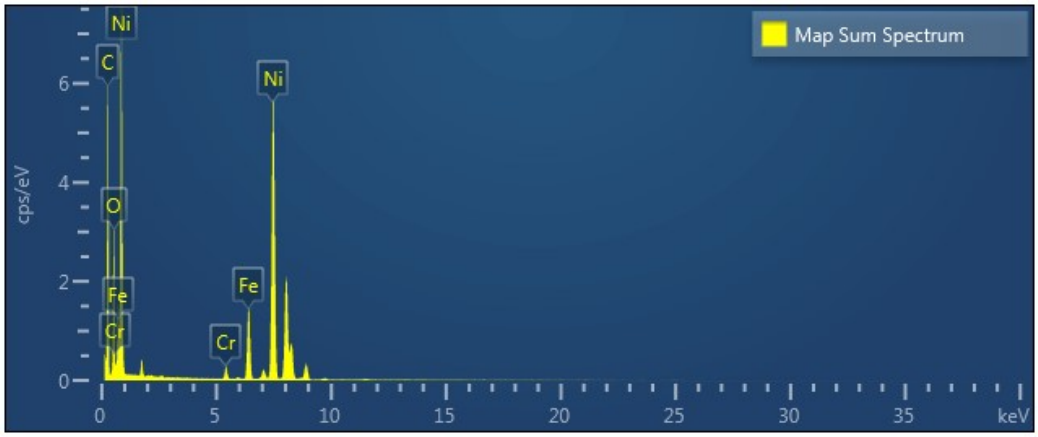

Fig. S5 EDX spectrum from HAADF-STEM of Cr-NiFe-MOF.

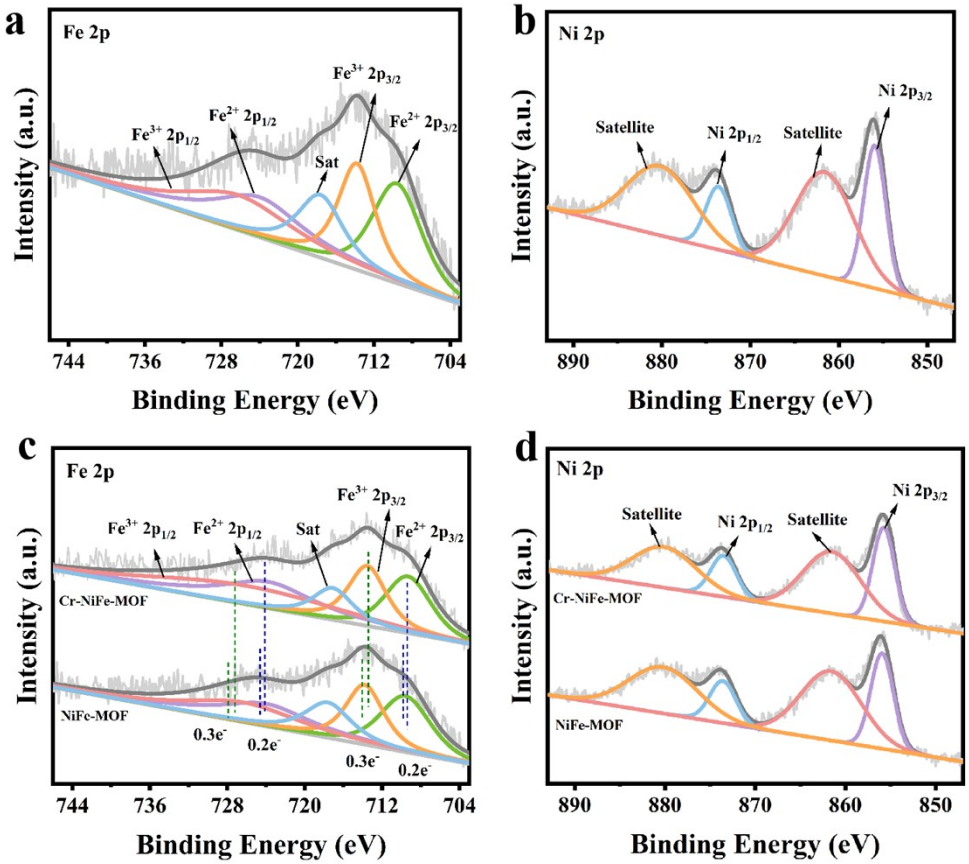

Fig. S6 XPS spectra of (a) Fe 2p of NiFe-MOF; (b) Ni 2p of NiFe-MOF; (c) Fe 2p of Cr-NiFe-MOF and NiFe-MOF; (d) Ni 2p of Cr-NiFe-MOF and NiFe-MOF.

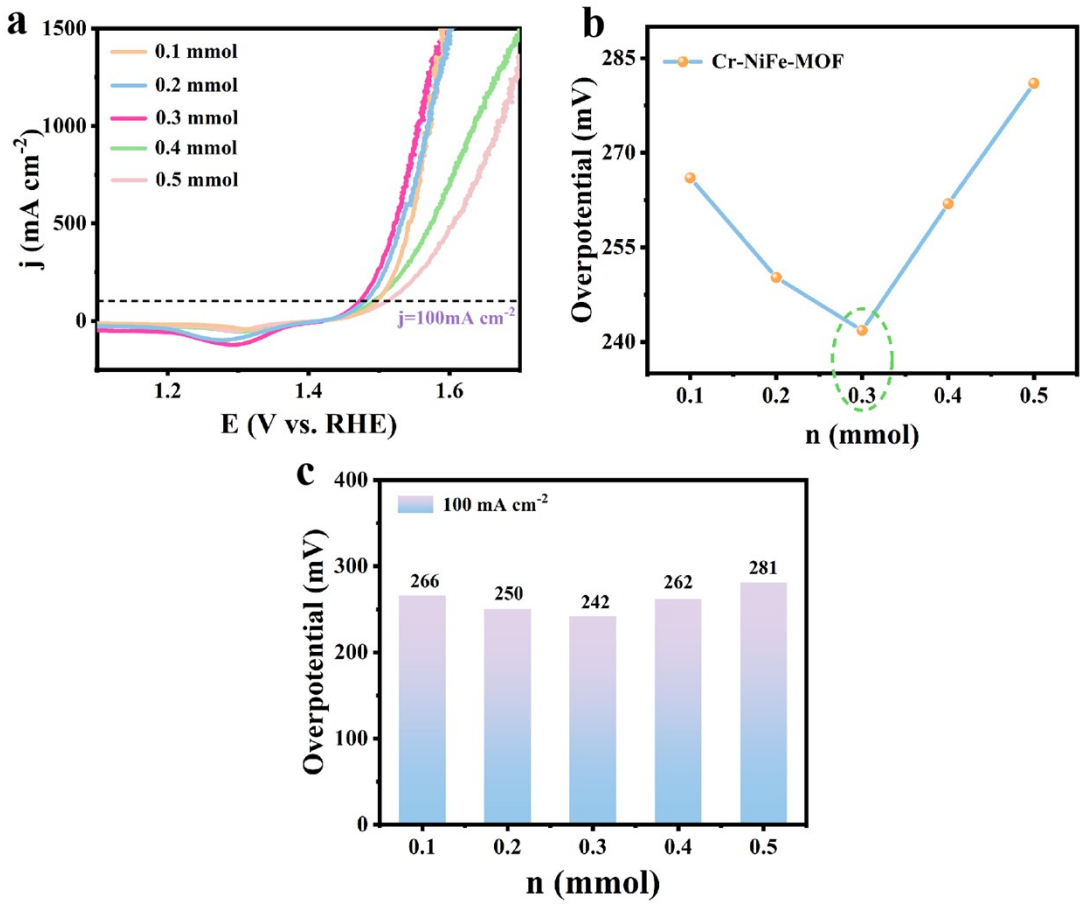

Fig. S7 (a) LSV curves and (b,c) comparison of the overpotential of different Cr contents of Cr-doped NiFe-MOF at 100 mA cm^{-2}.

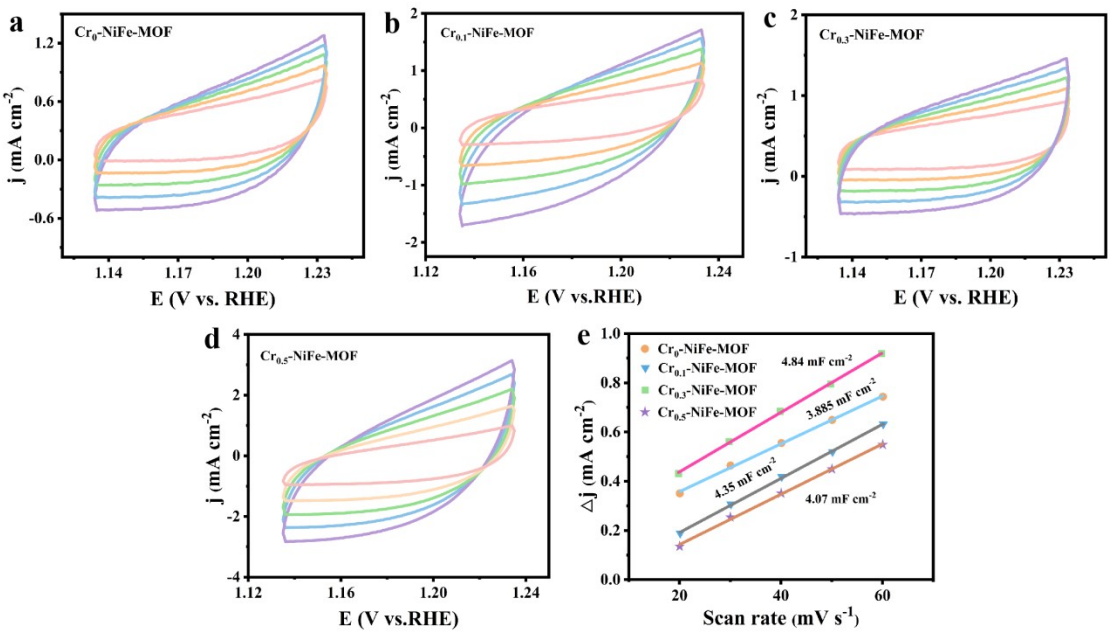

Fig. S8 CVs and C_{dl} value for Cr-NiFe-MOF of different Cr contents.

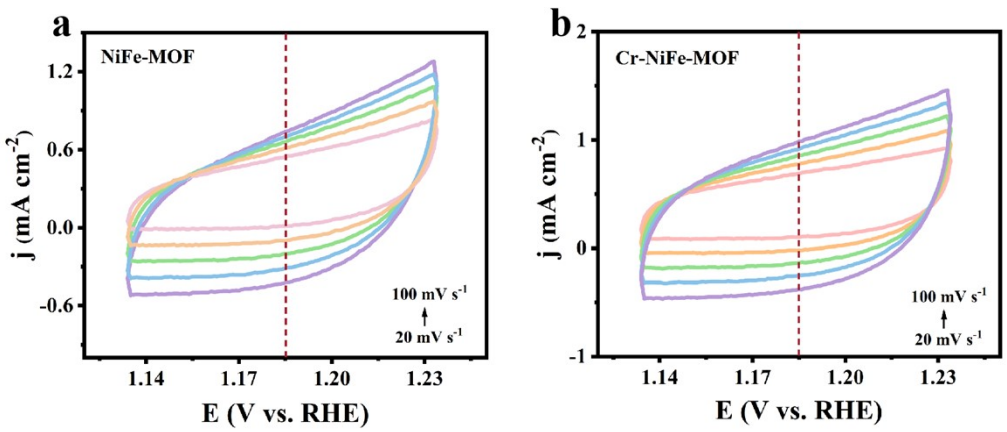

Fig. S9 CVs collected at various scan rates (20, 40, 60, 80 and 100 mV/s) for (a) NiFe-MOF, (b) Cr-NiFe-MOF in 1.0 M KOH.

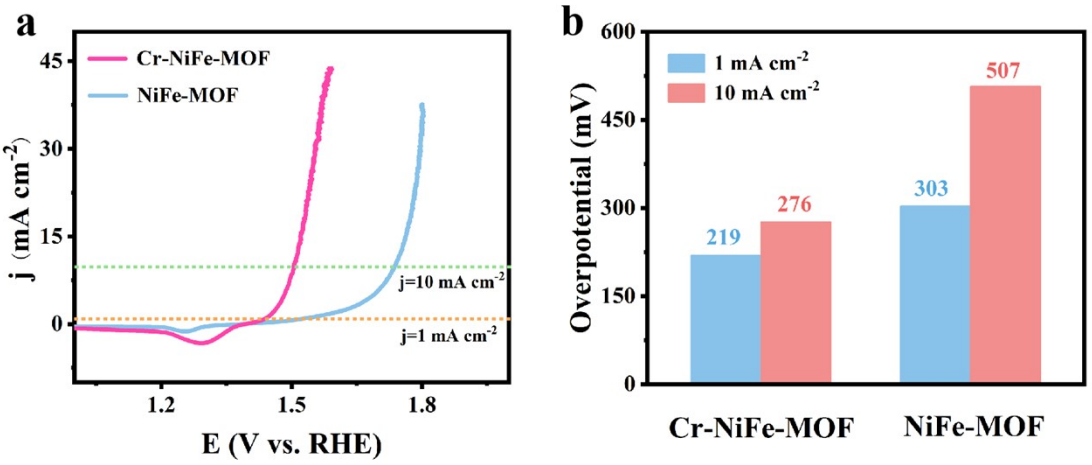

Fig. S10 (a) Polarization curves of catalysts based on ECSA; (b) Comparison of intrinsic OER electrocatalytic activities in the term of overpotentials required to reach an ECSA normalized current density of 1 and 10 mA cm^{-2}.

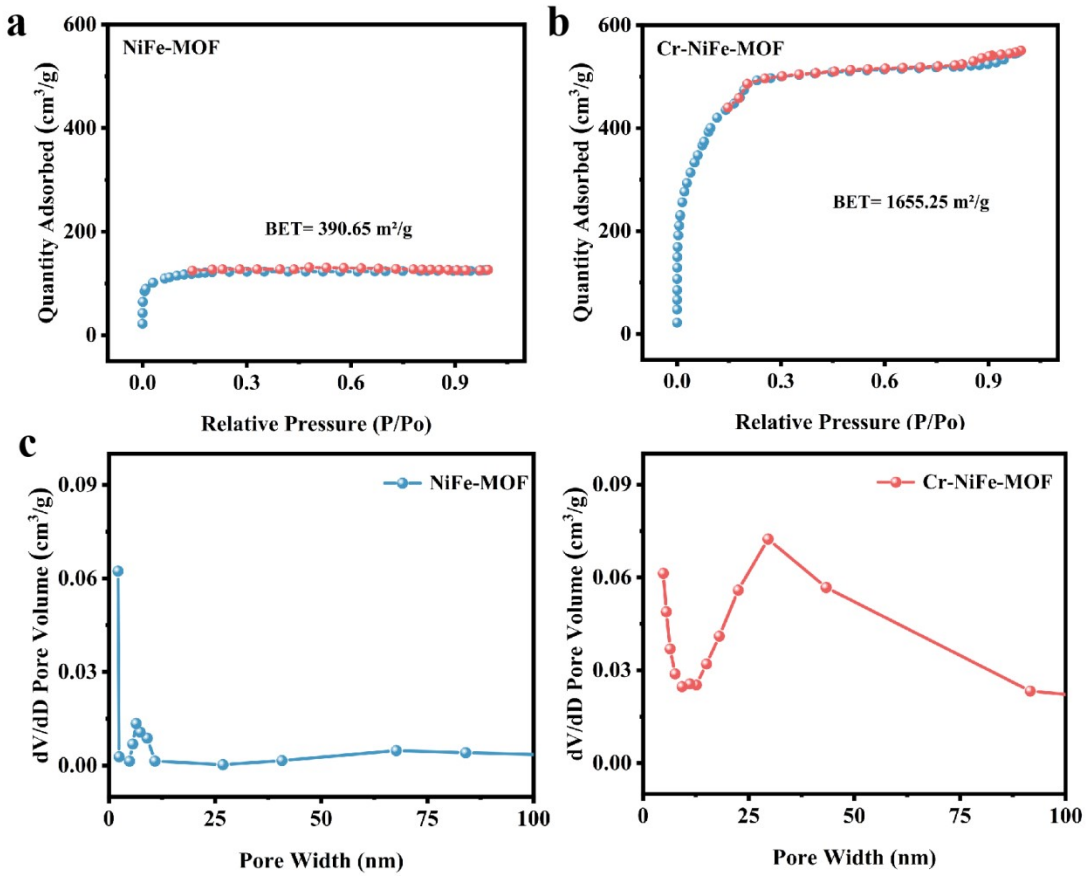

Fig. S11 N_2 sorption isotherms at 77 K for (a) NiFe-MOF and (b) Cr-NiFe-MOF. Pore size distribution of the (c) NiFe-MOF and (d) Cr-NiFe-MOF.

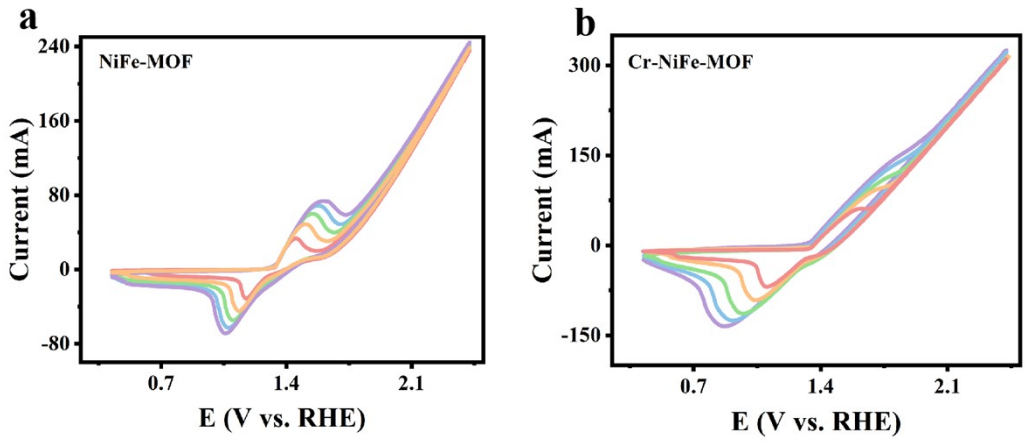

Fig. S12 CVs with different scan rates (20, 40, 60, 80 and 100 mV/s) in 1.0 M KOH of (a) NiFe-MOF and (b) Cr-NiFe-MOF.

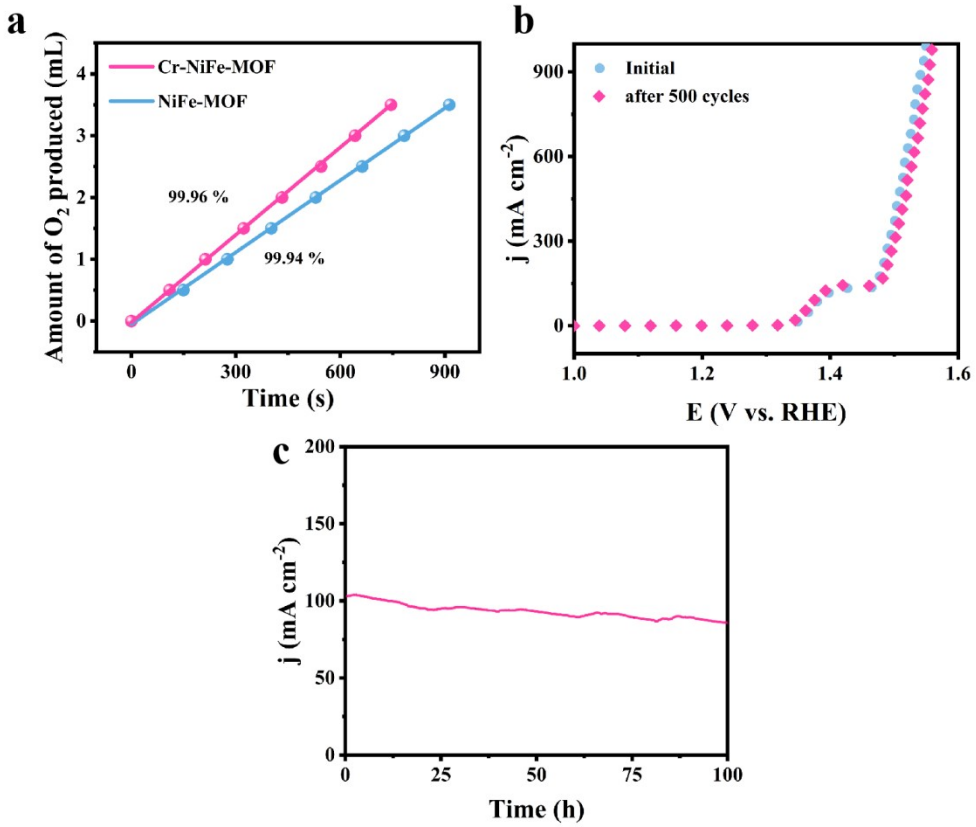

Fig. S13 (a) O_2 production from Cr-NiFe-MOF and NiFe-MOF at 100 mA cm^{-2}. (b) LSV curves of Cr-NiFe-MOF before and after 500 cycles. (c) Long-term stability test in 1.0 M KOH.

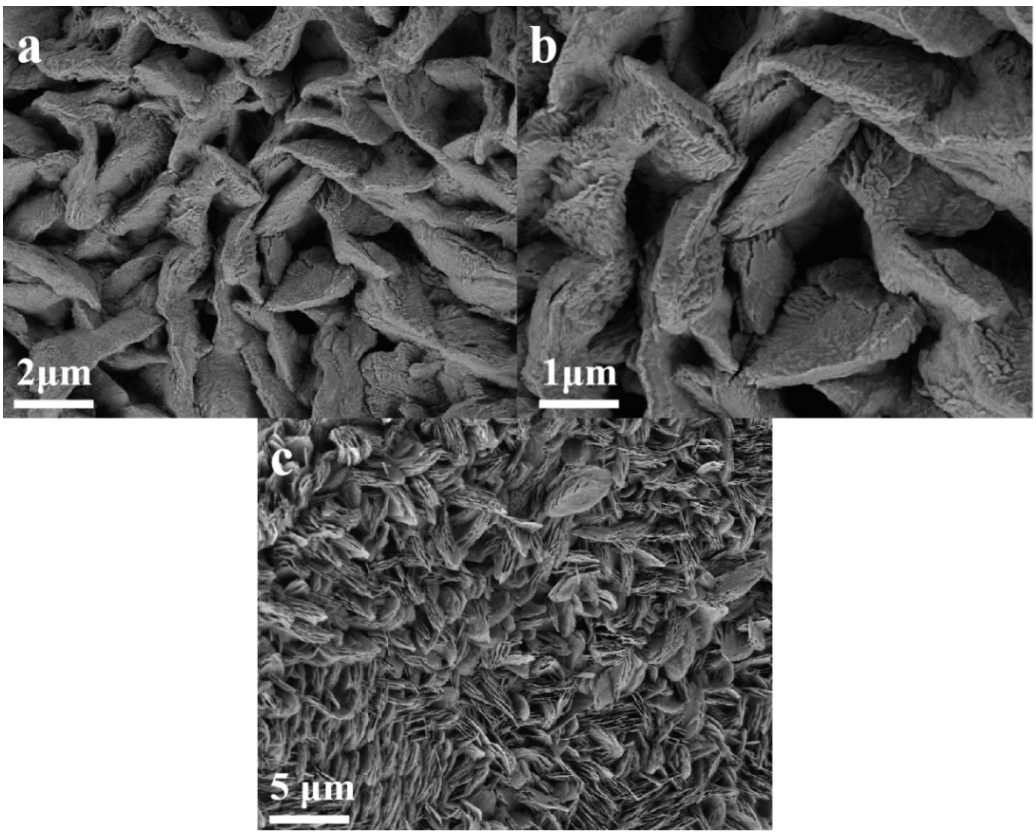

Fig. S14 The morphology characterizations of Cr-NiFe-MOF after stability test.

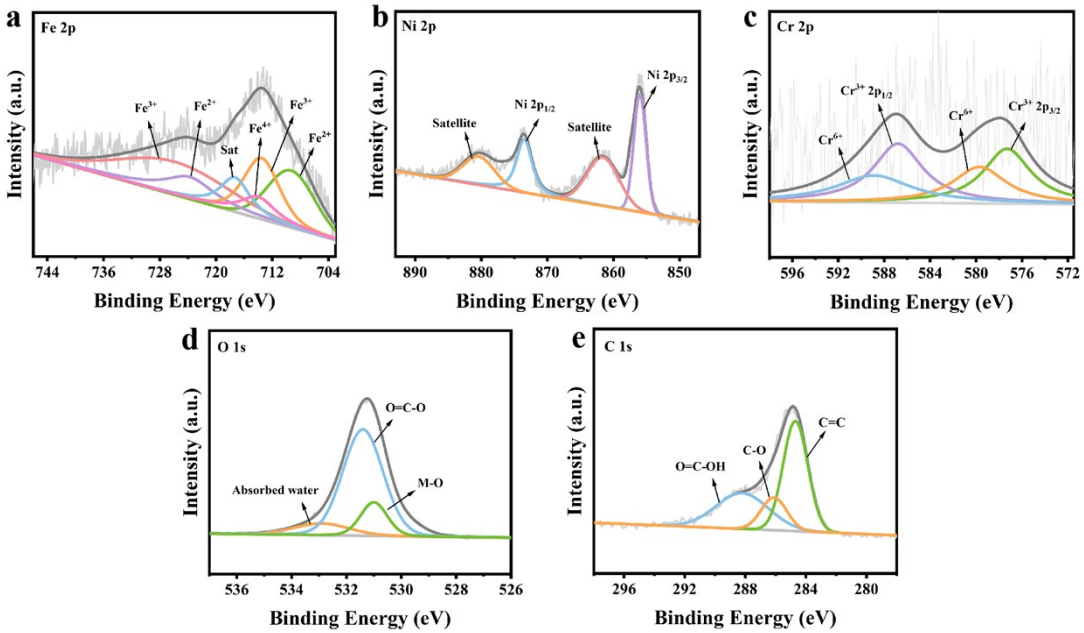

Fig. S15 XPS analysis of Cr-NiFe-MOF after stability test: (a) Fe 2p, (b) Ni 2p, (c) Cr 2p, (d) O 1s and (e) C 1s.

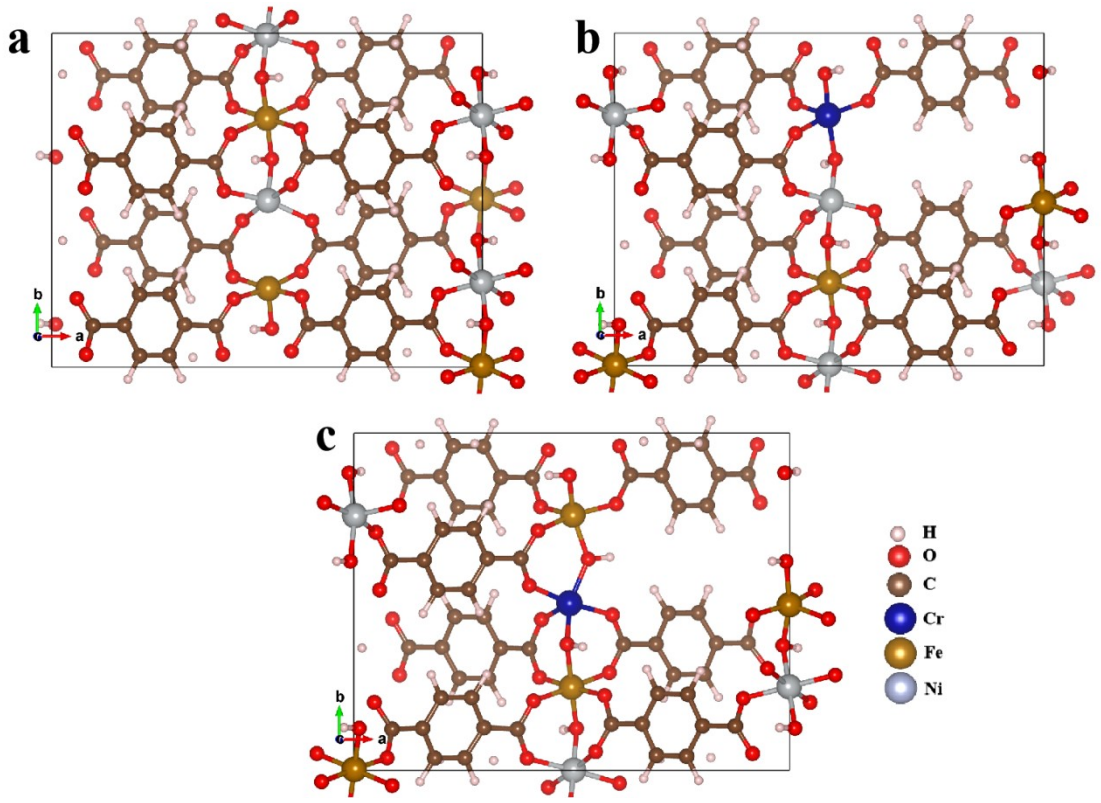

Fig. S16 Structural models of (a) original NiFe-MOF, (b) Cr replacing Fe site and (c) Cr replacing Ni site.

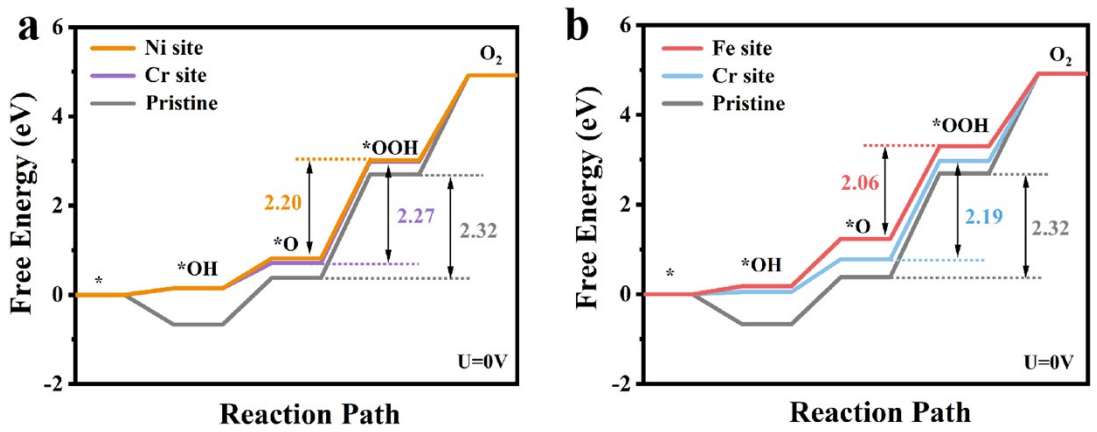

Fig. S17 Standard Gibbs free energy diagrams of OER key steps for Cr-NiFe-MOF in the case of (a) Cr replacing Fe site and (b) Cr replacing Ni site.

Table S1. Comparison of catalytic performance for Cr-NiFe-MOF with other reported OER at 100 mA cm^{-2}.

Catalyst	j (mA cm^{-2})	η (mV)	Electrolyte	Ref.
Cr-NiFe-MOF	100	242	1.0 M KOH	This work
NiFe-MOF	100	321	1.0 M KOH	This work
CoB_2O_4@FeOOH/NF	100	255	1.0 M KOH	7
NiFe LDH@SnO_2/NF	100	249	1.0 M KOH	8
NiCo-300	100	390	1.0 M KOH	9
$FeWO_4$-WO_3/NF	100	250	1.0 M KOH	10
KT-Ni(0)@Ni(II)-TPA	100	254	1.0 M KOH	11
CoMoP/CoP/NF	100	308	1.0 M KOH	12
MnCoP/NF	100	415	1.0 M KOH	13
FeOOH-a@NiFe LDHs	100	252	1.0 M KOH	14
$Fe_XNi_{2-X}P_4O_{12}$/RGO	100	277	1.0 M KOH	15
$CoCeNiFeZnCuO_X$	100	307	1.0 M KOH	16
Mo-NiOOH	100	390	1.0 M KOH	17

Ni_4Fe_1 LDH-16h/Ni-1000s@NF	100	270	1.0 M KOH	18
FeLDH(FeCo) on $Co(OH)_2$	100	279	1.0 M KOH	19
$FeCoNiS_X$	100	255	1.0 M KOH	20
Fe_3O_4@$NiCo_2O_4$	100	246	1.0 M KOH	21
$NiFe(OH)_X$@Ni_3S_2/MoS_2-CC	100	309	1.0 M KOH	22
NiCo/Ni/CuO/CF	100	286	1.0 M KOH	23
$Ni_{12}P_5$–Fe_2P–NbP	100	280	1.0 M KOH	24

Reference

1 G. Mu, G. Wang, Q. Huang, Y. Miao, D. Wen, D. Lin, C. Xu, Y. Wan, F. Xie, W. Guo and R. Zou, Adv. Funct. Mater., 2023, 33 2211260.

2 G. Kresse and J. Furthmüller, Phys. Rev. B., 1996, 6, 15-50.

3 P. E. Blöchl, Phys. Rev. B., 1994,50, 17953-17979.

4 J. P. Perdew, J. A. Chevary, S. H. Vosko, K. A. Jackson, M. R. Pederson, D. J. Singh asnd C. Fiolhais, Phys. Rev. B., 1992, 46, 6671-6687.

5 S. Grimme, J. Antony, S. Ehrlich and H. Krieg, J. Chem. Phys., 2010, 132, 154104.

6 J. Rossmeisl, A. Logadottir and J. K. Nørskov, Chem. Phys., 2005, 319, 178-184.

7 X. Yin, R. Cai, X. Dai, F. Nie, Y. Gan, Y. Ye, Z. Ren, Y. Liu, B. Wu and Y. Cao, J. Mater. Chem. A., 2022, 10, 11386-11393.

8 C. Wan, J. Jin, X. Wei, S. Chen, Y. Zhang, T. Zhu and H. Qu, J. Mater. Sci. Technol., 2022, 124, 102-108.

9 B. Zhang, X. Zhang, Y. Wei, L. Xia, C. Pi, H. Song, Y. Zheng, B. Gao, J. Fu and P.K. Chu, J. Alloys. Compd., 2019,797, 1216-1223.

10 F. Shen, Z. Wang, Y. Wang, G. Qian, M. Pan, L. Luo, G. Chen, H. Wei and S. Yin, Nano. Res., 2021, 14, 4356-4361.

11 Q. Hu, Z. Wang, X. Huang, Y. Qin, H. Yang, X. Ren, Q. Zhang, J. Liu, M. Shao and C. He, Appl. Catal. B., 2021, 286, 119920.

12 Y. Wei, W. Li, D. Li, L. Yi and W. Hu, Int. J. Hydrog. Energy, 2022, 47, 7783-7792.

13 W.-Y. Fu, Y.-X. Lin, M.-S. Wang, S. Si, L. Wei, X.-S. Zhao and Y.-S. Wei, Rare Metals, 2022, 41, 3069-3077.

14 M. Zhao, Y. Wang, W. Mi, J. Wu, J.-J. Zou, X.-D. Zhu, J. Gao and Y.-C. Zhang, Electrochimi. Acta. 2023, 458, 142513.

15 L. Lin, Y. Wang, Q. Ye, Y. Zhao and Y. Cheng, Appl. Catal. B., 2023, 334, 122834.

16 W. Huang, J. Zhang, D. Liu, W. Xu, Y. Wang, J. Yao, H.T. Tan, K.N. Dinh, C. Wu and M. Kuang, ACS. nano., 2020, 14, 17640-17651.

17 Y. Jin, S. Huang, X. Yue, C. Shu and P.K. Shen, Int. J. Hydrog. Energy, 2018, 43, 12140-12145.

18 Q. Yan, L. Kong, X. Zhang, T. Wei, J. Yin, K. Cheng, K. Ye, K. Zhu, J. Yan and D. Cao, Int. J. Hydrog. Energy, 2020, 45, 3986-3994.

19 F. Kong, W. Zhang, L. Sun, L. Huo and H. Zhao, ChemSusChem, 2019, 12, 3592-3601.

20 A. Wang, X. Zhang, S. Gao, C. Zhao, S. Kuang, S. Lu, J. Niu, G. Wang, W. Li and D. Chen, Adv. Mater., 2022, 34, 2204247.

21 Y. Jo, S. Cho, J. Seo, A.T.A. Ahmed, C.H. Lee, J.H. Seok, B. Hou, S.A. Patil, Y. Park and N.K. Shrestha, ACS. Appl. Mater., 2021, 13, 53725-53735.

22 X.H. Wang, Y. Ling, B.L. Li, X.L. Li, G. Chen, B.X. Tao, L.J. Li, N.B. Li and H.Q. Luo, J. Mater. Chem. A., 2019, 7, 2895-2900.

23 X. Wu, H. Lee, H. Liu, L. Lu, X. Wu and L. Sun, Int. J. Hydrog. Energy. 2020, 45, 21354-21363.

24 S. Wen, G. Chen, W. Chen, M. Li, B. Ouyang, X. Wang, D. Chen, T. Gong, X. Zhang and J. Huang, J. Mater. Chem. A., 2021, 9, 9918-9926.